

Enhancing Visual Inspection Capability of Multi-Modal Large Language Models on Medical Time Series with Supportive Conformalized and Interpretable Small Specialized Models

Huayu Li, Xiwen Chen, Ci Zhang, Stuart F. Quan,
William D.S. Killgore, Shu-Fen Wung, Chen X. Chen, Geng Yuan, Jin Lu, Ao Li

Abstract—Large language models (LLMs) exhibit remarkable capabilities in visual inspection of medical time-series data, achieving proficiency comparable to human clinicians. However, their broad scope limits domain-specific precision, and proprietary weights hinder fine-tuning for specialized datasets. In contrast, small specialized models (SSMs) excel in targeted tasks but lack the contextual reasoning required for complex clinical decision-making. To address these challenges, we propose ConMIL (Conformalized Multiple Instance Learning), a decision-support SSM that integrates seamlessly with LLMs. By using Multiple Instance Learning (MIL) to identify clinically significant signal segments and conformal prediction for calibrated set-valued outputs, ConMIL enhances LLMs’ interpretative capabilities for medical time-series analysis. Experimental results demonstrate that ConMIL significantly improves the performance of state-of-the-art LLMs, such as ChatGPT4.0 and Qwen2-VL-7B. Specifically, ConMIL-supported Qwen2-VL-7B achieves 94.92% and 96.82% precision for confident samples in arrhythmia detection and sleep staging, compared to standalone LLM accuracy of 46.13% and 13.16%. These findings highlight the potential of ConMIL to bridge task-specific precision and broader contextual reasoning, enabling more reliable and interpretable AI-driven clinical decision support.

Index Terms—Medical time series, Healthcare AI, Multimodal Large language model, Clinical Decision Support

I. INTRODUCTION

Medical time series, such as electrocardiograms (ECGs) and electroencephalograms (EEGs), offer a wealth of information about a patient’s health status through sequentially sampled physiological signals. Traditionally, clinicians have relied on visual inspection to interpret these signals, identifying trends and anomalies that guide diagnoses and treatment decisions. However, this manual process is time-intensive and prone to human error, especially in complex cases or under high workload conditions. Artificial Intelligence (AI) has emerged as a powerful tool to address these challenges, enabling automated interpretation of medical time series. For clinicians, AI systems offer efficiency and accuracy by processing vast amounts of complex data and detecting critical patterns that may elude human observers. For patients, these systems can lead to earlier disease detection and more personalized care, particularly in underserved regions.

Despite these benefits, existing AI solutions face limitations. Small specialized models (SSMs) [1]–[6] are task-focused and small-scale architectures designed for specific tasks such as arrhythmia detection or sleep stage classification. SSMs are the mainstream of medical time series domain which usually directly process the raw time series data. SSMs excel in their narrow domains but lack the broader reasoning capabilities required for complex clinical decision-making. On the other hand, large language models (LLMs) have rapidly gained traction in healthcare [7]–[9]. The ability of LLMs to process visual-language tasks enable them performs medical time series interpretation by visual inspection [10]–[14] with reasoning processes that mimic human clinicians. LLMs hold the promise of context-aware, intuitive decision-making, but their broad scope comes with drawbacks: limited domain-specific precision, high computational costs for fine-tuning, and restricted accessibility due to proprietary weights.

These contrasting strengths and weaknesses reveal a significant opportunity: *How can we combine the task-specific expertise of SSMs with the contextual reasoning capabilities of LLMs to enable robust, interpretable, and reliable visual inspection for medical time series?* To address this, we must reconsider the role of SSMs in the medical time series domain. Rather than functioning as standalone predictors, SSMs can be reimagined as specialized, complementary modules that enhance the reasoning capabilities of LLMs. This reframing leads to a central question: *How can we effectively integrate SSMs into the LLM workflow to maximize their utility while addressing their inherent limitations?* Achieving this synergy requires a thoughtfully designed framework that aligns with clinical workflows and ensures that the outputs of SSMs are both interpretable and actionable. By embedding the insights of SSMs into the LLM decision-making process, we can enable more informed, transparent, and collaborative clinical decisions, bridging the gap between task-specific precision and broad, context-aware reasoning.

A critical consideration is how to use the predictions of SSMs to guide LLMs in their decision-making. Ideally, SSMs should reduce the likelihood of errors made by LLMs by providing higher prediction accuracy on specialized tasks.

However, in practice, SSMs may not always surpass the accuracy of LLMs, even when trained specifically on medical time series data. Erroneous predictions from SSMs could potentially mislead LLMs, undermining their decision-making rather than enhancing it. Furthermore, when SSM and LLM predictions conflict, it can be difficult for users to determine which model to trust. Beyond merely generating predictions, SSMs should offer deeper insights into the medical time series data, enabling LLMs to validate and contextualize their outputs. This highlights the need for an integrated approach that ensures both interpretability and reliability, empowering LLMs to make more accurate and trustworthy clinical decisions.

To address these limitations, we need approaches that offer both interpretability and uncertainty quantification. One promising strategy is the integration of Multiple Instance Learning (MIL) and conformal prediction. MIL is a weakly supervised learning technique that treats medical time series data as collections of instances, such as individual time segments. It identifies which segments have most influence on a given classification or prediction [5], [6]. This detailed perspective not only enhances transparency but also allows LLMs to validate predictions by tracing them back to specific, clinically meaningful intervals. However, while MIL excels at interpretability, it does not inherently quantify uncertainty. Conformal prediction addresses this gap by producing set-valued predictions at predefined confidence levels [15], thereby providing a clear measure of reliability. By combining MIL’s interpretability with conformal prediction’s reliability, we create a compelling paradigm that can bolster both transparency and trustworthiness. Ultimately, this integration can transform SSMs into safer and more actionable supportive plug-in for visual inspection of LLMs on medical time series.

We introduce **ConMIL (Conformalized Multiple Instance Learning)**, a supportive SSM to enhance the visual inspection capabilities of LLMs on Medical time series data. **ConMIL** offers two main advantages: First, unlike conventional MIL methods that only handle single positive class (e.g., single diagnosis), we proposed *QTrans-Pooling* mechanism. This mechanism uses learnable class tokens and cross-attention to identify the most salient data segments for each class, facilitating intuitive understanding. This is particularly beneficial in scenarios with multiple diagnoses, outcomes, or treatment options. Second, **ConMIL** incorporates conformal prediction to deliver class-specific confidence measures by dynamically adjusting prediction thresholds based on calibration sets. This approach ensures that every reported prediction is supported by a rigorously quantified level of reliability. To our knowledge, **ConMIL** is the first to combine conformal prediction with MIL, marking a notable advancement in healthcare AI.

Crucially, **ConMIL** embodies a strategic shift in how SSMs enhance clinical decision-making by leveraging LLMs for visual inspection of medical time series data. By providing interpretable, confidence-calibrated set-valued outputs, **ConMIL** reduces the risk of misdiagnoses and misclassifications compared to opaque black-box models. The synergy between MIL’s interpretability and conformal prediction’s uncertainty

quantification is designed to meet the demands of high-stakes healthcare contexts. Through comprehensive evaluations, including sleep stage and arrhythmia classification (see Section V-C), we demonstrate that integrating **ConMIL** with LLMs substantially improves diagnostic accuracy. These findings underscore the importance of combining interpretability and set-valued prediction to advance reliable and effective AI-informed clinical decision support.

II. RELATED WORKS

A. Medical Time Series Classification

Medical time series, such as ECG and EEG signals, are critical for monitoring health, diagnosing diseases, and predicting clinical outcomes. Tasks like detecting arrhythmias from ECG [16], predicting seizures from EEG [17], and classifying sleep stages [18] rely on accurate classification. While traditional approaches used feature engineering and classical machine learning [19], [20], deep learning models, including CNNs [3], [21]–[23], and transformer-based architectures [4], [24]–[26] now dominate the field due to their ability to handle complex temporal patterns.

B. Time Series Multiple Instance Learning (MIL)

MIL addresses tasks where labels exist at the bag level, with only some instances within a bag relevant to the label [27]. Applied to time series, MIL identifies critical segments that contribute to classification [5], [6], making it highly interpretable and effective in noisy medical data. Unlike post-hoc interpretation methods such as SHAP [28] or LIME [29], MIL directly integrates interpretability into the modeling process, ensuring robust performance and precision in high-stakes domains like healthcare.

C. Conformal Prediction

Conformal prediction [15] offers set-valued predictions with predefined coverage, ensuring rigorous uncertainty quantification. Its adaptability to complex tasks like MIL remains underexplored but holds promise for enhancing reliability and interpretability in medical time series classification. Compared to Bayesian approaches [30] or Monte Carlo dropout [31], conformal prediction guarantees valid coverage, is computationally efficient, and is non-parametric, making it particularly suited for medical applications where accuracy and interpretability are critical.

D. Clinical Decision-Making with LLMs

LLMs are transforming clinical decision-making by supporting diagnostics, treatment recommendations, and risk assessment. Models like Med-PaLM [8] have demonstrated near-expert-level performance in standardized exams through domain-specific pre-training and structured prompts. These models excel in nuanced medical reasoning, including step-by-step diagnostic queries, and have shown promise in analyzing visual data like ECGs [10] and supporting applications in sleep medicine [9]. The integration of LLMs into clinical workflows enhances accuracy, reduces cognitive load, and broadens AI’s utility in healthcare.

III. CONFORMALIZED MULTIPLE INSTANCE LEARNING

This section delves into the motivations, foundational principles, and algorithmic underpinnings of **ConMIL**, providing a comprehensive explanation of its design and technical validity.

A. Problem Formulation

We first formulate the problem of time series classification in the context of medical data. Given a time series input $X = [x_1, x_2, \dots, x_T]$, where each $x_t \in \mathbb{R}^n$ represents a n -variate feature vector recorded at time t , the goal is to assign the correct class label $y \in \mathcal{Y} = \{1, \dots, K\}$ from K possible classes. These classes may represent different medical conditions or diagnostic categories, such as arrhythmia types, sleep stages, or seizure events.

Time series classification can naturally be formulated as a MIL problem by treating each time series as a “bag”, where each time step is considered an instance. In conventional MIL, the model learns a binary mapping $f : X \rightarrow \hat{y}$, which aggregates information across all instances within the bag to predict the bag-level label. This can be formally defined as:

$$\hat{y}_i = \begin{cases} 0, & \text{iff } \sum_{t=1}^T \hat{y}_i^t = 0, \hat{y}_i^t \in \{0, 1\} \\ 1, & \text{otherwise,} \end{cases} \quad (1)$$

where \hat{y}_i^t represents the instance-level label at time point, indicating whether an event of interest has occurred at that time step x_i^t . For a multi-class classification problem with K classes, time series classification can be extended by performing several *one-vs-rest* binary MIL tasks without violating the assumptions of MIL. Formally, this is defined as:

$$\hat{y}_{i,k} = \begin{cases} 0, & \text{iff } \sum_{t=1}^T \hat{y}_{i,k}^t = 0, \hat{y}_{i,k}^t \in \{0, 1\} \\ 1, & \text{otherwise,} \end{cases} \quad (2)$$

where $\hat{y}_{i,k}^t$ denotes the instance-level label at time point t , representing the contribution to class $k \in \{1, \dots, K\}$. The final bag-level prediction is determined by selecting the class with the highest probability, indicated by $\hat{y}_i = \arg \max_k \hat{y}_{i,k}$.

Conformal prediction is a framework designed to provide reliable uncertainty estimates for model predictions. Instead of outputting a single predicted label, conformal prediction generates a set-valued prediction that contains the true label with a user-defined probability, known as the *coverage*. In medical settings, for instance, conformal prediction can offer a set of possible diagnoses, guaranteeing that the correct diagnosis is included in this set with at least $1 - \alpha$ confidence, where α represents the error rate or miscoverage rate. Formally, given the ground truth label y , the input time series, our goal is to construct a set-valued prediction $\mathcal{S}_\alpha(X) \subseteq \mathcal{Y}$ such that:

$$\mathbb{P}(y \in \mathcal{S}_\alpha(X)) \geq 1 - \alpha, \quad (3)$$

for a pre-specified miscoverage rate, such as 10%.

B. *Q*Trans-Pooling with per-class interpretability

We first recap the approximation of the general MIL methods stated in [32], [33],

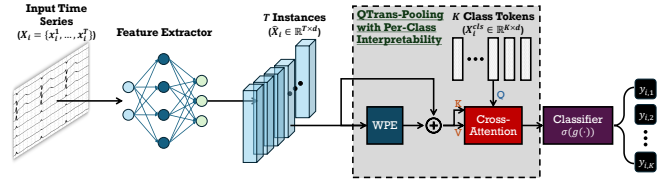


Fig. 1. Illustration of the MIL model used in **ConMIL**. Our model is adapted from the one proposed by [5] which uses InceptionTime [3] as the feature extractor and encodes temporal correlations with Wavelet Positional Encoding (WPE) [5]. Instead of *Trans-Pooling*, we have introduced the *Q*Trans-Pooling for enhanced per-class interpretability.

Theorem 1. Suppose the score function S is a $(\delta_\varepsilon, \varepsilon)$ -continuous symmetric function w.r.t Hausdorff distance $d_H(\cdot, \cdot)$. For any invertible map $\psi : \mathcal{X} \rightarrow \mathbb{R}^d$, S can be approximated by certain continuous functions g and f :

$$|S(X_i) - g(\psi\{\phi(x_i^t) : x_i^t \in X_i\})| < \varepsilon, \quad (4)$$

where x_i^t denotes the t th instance of the bag X_i .

This theorem presents the pipeline of MIL paradigm that existing architectures typically consist of three main components: 1) a feature extractor $\phi(\cdot)$, which processes the input time series X and extracts a set of d -dimensional feature embeddings $Z \in \mathbb{R}^{T \times d} = [z_1, z_2, \dots, z_T]$; 2) a MIL pooling layer $\psi(\cdot)$, which computes a weighted feature vector $Z^{pool} \in \mathbb{R}^d$ along with corresponding attention weights $A = [a_1, a_2, \dots, a_T]$, where $a_t \in \{0, 1\}$, for each instance, offering interpretability by highlighting the contributions of individual time steps to the final decision; and 3) a classifier $g(\cdot)$ which takes the pooled feature vector Z^{pool} as input and outputs class probabilities. Formally, the MIL can be formulated as following general process:

$$Z = \phi(X), \{Z^{pool}, A\} = \psi(Z), \hat{y} = g(Z^{pool}) \quad (5)$$

Our study begins by examining the limitations of two recent MIL methods—Conjunctive Pooling [6] and *Trans-Pooling* [5]—within the context of time series analysis. Conjunctive pooling [6] is a novel pooling method that independently applies instance-wise attention and classification to the time point embeddings, followed by scaling the time point predictions using the corresponding attention values. Slightly different from the general process, conjunctive pooling is defined as:

$$\hat{y}_t = g(z_t), \hat{y} = \frac{1}{T} \sum_{t=0}^T (a_t \hat{y}_t), a_t \in \{0, 1\} = \sigma(W^A z_t). \quad (6)$$

In this formulation, a_t is the attention value assigned to each time point t , calculated by applying a sigmoid activation σ to the feature vectors $W^A z_t$.

On the other hand, *Trans-Pooling* [5] introduces the use of Transformers [24] in MIL, leveraging their self-attention mechanism to capture dependencies between a learnable class

token z^{cls} and each instance. Formally, the process is defined as:

$$\begin{aligned}\hat{y} &= g(\hat{z}^{\text{cls}}), \\ \hat{Z} &= \text{Attention}(W^Q Z^{\text{cls}}, W^K Z^{\text{cls}}, W^V Z^{\text{cls}}) W^O \\ &= [\hat{z}^{\text{cls}}, \hat{z}_1, \dots, \hat{z}_T],\end{aligned}$$

where W^Q , W^K , W^V , and W^O are trainable parameters, the self-attention mechanism is computed as:

$$\text{Attention}(Q, K, V) = \text{softmax}\left(\frac{QK^\dagger}{\sqrt{d}}\right)V, \quad (7)$$

and $\hat{Z} = [z^{\text{cls}}, z_1, \dots, z_T]$ is the concatenation of the class token z^{cls} and the instance embeddings z_1, \dots, z_T . The attention mechanism enables the model to weigh the importance of each instance in relation to the class token, refining the pooled representation \hat{z}^{cls} for final classification.

We observed that these while both methods were helpful, they did not fully meet our objective of per-class interpretability. These methods focus on providing insight into the model’s final prediction by identifying which time steps are most influential to the overall classification. However, they do not offer insights into the contributions of individual time steps for each potential class. In other words, while the attention mechanisms in both conjunctive pooling and *Trans-Pooling* provide useful explanations for the final decision, they do not offer a breakdown of how each instance relates to every possible class in multi-class classification tasks.

To address this, we proposed the *QTrans-Pooling* used in **ConMIL** as illustrated in Fig. 1. Inspired by the work of [5], we also implement *QTrans-Pooling* with learnable class tokens and Transformers. Considering the instance importance can be measured by the attention maps between class tokens and instances, to achieve per-class interpretability can be implemented via assigning each class an independent class token. To this end, we introduce a separate class token z_k^{cls} , allowing the model to compute class-specific attention weights for each instance. In *QTrans-Pooling*, cross-attention between the class tokens and instance embeddings used to achieve per-class interpretability. Given the class tokens $Z^{\text{cls}} = [z_1^{\text{cls}}, \dots, z_k^{\text{cls}}]$, and instance embeddings $Z = [z_1, \dots, z_T]$, the cross-attention is computed as follows:

$$\text{Attention}(Q, K, V) = \sigma\left(\frac{QK^\dagger}{\sqrt{d}} + b\right)V, b = -\log(T), \quad (8)$$

with $Q = W^Q Z^{\text{cls}}$, $K = W^K Z$, $V = W^V Z$. The bias term is defined as b and σ is the Sigmoid function. Sigmoid attention [34] is used since the softmax function may possibly cause attention to focus on a few features while ignoring other information. This process allows the class token z_k^{cls} to attend to the embeddings of the instance, resulting in an attention map $A_k = [a_{k,1}, a_{k,2}, \dots, a_{k,T}]$, where each $a_{k,t}$ represents the importance of time step t for class k .

The use of cross-attention between class tokens and instance embeddings is pivotal for achieving per-class interpretability. By assigning a distinct learnable class token to each class,

the model can independently compute the relevance of each instance to each class. This capability is particularly significant in multi-class medical time series classification tasks, where understanding the contribution of individual time segments to multiple potential diagnoses is critical for informed clinical decision-making. Moreover, the use of independent class tokens allows the model to disentangle overlapping features across different classes, resulting in more precise and interpretable predictions. For example, in ECG analysis, specific time segments may correspond to different heart rhythm abnormalities, and per-class tokens help clarify which signal features are relevant to each diagnosis. We further provide an information-theoretical justification to validate this property.

Theorem 2. *Compared with Trans-Pooling [5], applying QTrans-Pooling with Per-Class Interpretability may lower class-wise variability and hence reduce the complexity of developing a good classifier in latent space. We use class-conditioned entropy to describe the homogeneity of feature space in a specific class:*

$$H(\hat{Z}|z_1^{\text{cls}}, \dots, z_k^{\text{cls}}) \leq H(\hat{Z}|\hat{z}^{\text{cls}}), \quad (9)$$

where $H(\hat{Z}|z_1^{\text{cls}}, \dots, z_k^{\text{cls}})$ denotes modeling instances within a class with per-class token by our method while $H(\hat{Z}|\hat{z}^{\text{cls}})$ denotes modeling instances within a class with only one global token by Trans-Pooling.

Proof. The proof is straightforward, as conditioning on additional information can only maintain or lower the conditional information [35]. \square

Remark 1. *A reduction in class-conditioned entropy implies that features within the same class form tighter clusters, thereby reducing variability between classes. Consequently, minimizing class-wise variability across all classes facilitates the identification of simpler and more robust decision boundaries for classification.*

Remark 2. *Lower class-conditioned entropy enhances confidence in assigning instances to their correct classes, improving classification reliability and interpretability.*

C. Conformalizing the MIL model

We now discuss how to achieve reliable set-valued prediction with per-class coverage guarantees by integrating conformal prediction into **ConMIL**. To this end, we aim to construct set-valued prediction that control the FNR for each class k , ensuring that the true class is included in the set-valued prediction with high probability. We consider implementing **ConMIL** under the split conformal prediction setting [36]. We reserve a dataset calibration dataset which remains unseen

during training the MIL model, we seek to construct a set-valued prediction $\mathcal{S}_\alpha(X_{\text{test}})$ of the new test data which is valid in the following sense:

$$\begin{aligned} \mathbb{P}(y_{\text{test}} \in \mathcal{S}_\alpha(X_{\text{test}}) | y_{\text{test}} = k) &\geq 1 - \alpha, \\ \forall k \in \{1, \dots, K\}, \end{aligned} \quad (10)$$

where α is the predefined confidence level and $\mathcal{S}_\alpha(X)$ represents the set-valued prediction for input X . This guarantees that for each class k , the true class is captured with at least $1 - \alpha$ probability, controlling the likelihood of missing a true positive (i.e., controlling the FNR).

For each class k , the FNR in a dataset $\mathcal{D} = \{(X_1, y_1), \dots, (X_N, y_N)\}$, where N represents the number of samples, can be defined in terms of a risk function. The risk function quantifies the empirical likelihood that the presence of class k is not correctly predicted in the data set. Formally, the risk for class k is defined as:

$$\mathcal{R}_k(\mathcal{D}) = 1 - \frac{1}{N} \sum_{i=0}^{N_k} \mathbb{I}(y_i \in \mathcal{S}_\alpha(X_i)), \quad (11)$$

where N_k is the number of samples in \mathcal{D} with true class label k , \mathbb{I} is the indicator function that equals 1 if the condition is satisfied and 0 otherwise, $y_i \in \mathcal{S}_\alpha(X_i)$ indicates whether the true label is included in the set-valued prediction. In binary classification, the model's final prediction is often decided by thresholding the predicted probability with a predefined threshold λ . The binary prediction \hat{y}_i is determined by rounding the predicted probability $\hat{p}(X_i)$:

$$\hat{y}_i = \begin{cases} 1, & \text{if } \hat{p}(X_i) \geq 1 - \lambda, \\ 0, & \text{otherwise.} \end{cases} \quad (12)$$

The per-class FNR is controlled by selecting an appropriate threshold λ such that the set-valued prediction includes the true class label with the desired coverage probability. To generalize this for multi-class classification, we assign a threshold λ_k for each class k , forming a set of thresholds $\lambda = \{\lambda_1, \dots, \lambda_K\}$. These thresholds act as additional parameters for constructing the set-valued prediction $\mathcal{S}_\alpha(X_i, \lambda)$, which is defined as:

$$\mathcal{S}_\alpha(X_i, \lambda) := \{\hat{y}_{i,k} : p(X_i) \geq 1 - \lambda_k\}. \quad (13)$$

This formulation ensures that the set-valued prediction includes all classes for which the predicted probability exceeds the class-specific threshold λ_k .

For picking the threshold λ , Conformal Risk Control (CRC) [37] is a natural choice, as it provides a principled framework for balancing coverage guarantees with risk control. CRC extends traditional conformal prediction by incorporating the notion of risk minimization, allowing us to adjust thresholds dynamically to ensure that the set-valued prediction achieves a predefined level of reliability while controlling FNRs across multiple classes.

Definition 1. (Conformal Risk Control [37]) Given an arbitrary bounded risk function $\mathcal{R}_\lambda(\cdot) \in (-\inf, B]$ for

some $B < \infty$ that is monotonically non-increasing with respect to the threshold λ , the goal of CRC is to select the smallest possible threshold such that the risk remains controlled at a predefined level. Formally, for a given calibration dataset \mathcal{D}_{cal} and a risk level α , CRC selects $\hat{\lambda}$ such that the risk on the test data $\mathcal{D}_{\text{test}}$ is controlled:

$$\mathbb{E}[\mathcal{R}_{\hat{\lambda}}(\mathcal{D}_{\text{test}})] \leq \alpha, \quad (14)$$

where the optimal threshold $\hat{\lambda}$ is selected by solving the following optimization problem:

$$\hat{\lambda} = \inf \left\{ \lambda : \frac{n}{n+1} \mathcal{R}_\lambda(\mathcal{D}_{\text{cal}}) + \frac{B}{n+1} \leq \alpha \right\} \quad (15)$$

where $\mathcal{R}_\lambda(\mathcal{D}_{\text{cal}})$ is the empirical risk based on the calibration data.

By using CRC, we are able to dynamically adjust the threshold λ on the calibration dataset to achieve the per-class coverage. To demonstrate that CRC provides guarantees, we first relax the assumption of independent and identically distributed (i.i.d.) data and instead consider an exchangeable data distribution.

Definition 2. (Exchangeable data distribution) Let \mathcal{X} and \mathcal{Y} represent the time series input and label space, respectively. A data distribution in $\mathcal{X} \times \mathcal{Y}$ is said to be exchangeable if and only if the following condition holds:

$$\begin{aligned} \mathbb{P}((X_{\pi(1)}, y_{\pi(1)}), \dots, (X_{\pi(N)}, y_{\pi(N)})) \\ = \mathbb{P}((X_1, y_1), \dots, (X_N, y_N)) \end{aligned} \quad (16)$$

for any finite sample $\{(X_n, y_n)\}_{n=1}^N$, where $\pi(\cdot)$ denotes an arbitrary permutation of the dataset indices.

Under the assumption of an exchangeable data distribution, CRC provides exact guarantees as stated in the following theorem.

Theorem 3. (Conformal risk control over exchangeable data distribution) Given a risk function \mathcal{R}_λ that is right-continuous and non-increasing with respect to λ , and a calibration dataset $\mathcal{D}_{\text{cal}} = \{\mathcal{D}_n\}_{n=1}^N$ containing N data points, we also denote any test point as \mathcal{D}_{N+1} . If the calibration and test datasets are sampled from an exchangeable distribution $\mathcal{X} \times \mathcal{Y}$, then the following conditions hold:

$$\begin{aligned} \mathcal{R}_{\lambda_{\max}}(\mathcal{D}_n) &\leq \alpha, \\ \sup_{\lambda} \mathcal{R}_\lambda(\mathcal{D}_n) &\leq B < \infty \text{ almost surely.} \end{aligned} \quad (17)$$

and thus,

$$\mathbb{E}[\mathcal{R}_{\hat{\lambda}}(\mathcal{D}_{N+1})] \leq \alpha. \quad (18)$$

where $\hat{\lambda}$ is the optimal threshold selected by CRC as per Eq. 15.

Proof. Let the risk over the union of the calibration set and a test point be denoted as:

$$\begin{aligned}\mathcal{R}_\lambda(\mathcal{D}_{U_n}) &= \mathcal{R}_\lambda(\mathcal{D}_{cal} \cup \mathcal{D}_{N+1}) \\ &= \frac{1}{N+1} \sum_{n=1}^{N+1} \mathcal{R}_\lambda(\mathcal{D}_n).\end{aligned}\quad (19)$$

We aim to find the smallest λ that satisfies:

$$\hat{\lambda}' = \inf \left\{ \lambda : \hat{\mathcal{R}}_\lambda(\mathcal{D}_{U_n}) \leq \alpha \right\}.\quad (20)$$

Given that $\inf_\lambda \mathcal{R}_\lambda(\mathcal{D}_n) = \mathcal{R}_{\lambda_{\max}}(\mathcal{D}_n) \leq \alpha$ and $\mathcal{R}_\lambda(\mathcal{D}_{N+1}) \leq B$, we can compute:

$$\begin{aligned}\mathcal{R}_\lambda(\mathcal{D}_{U_n}) &= \frac{N}{N+1} \mathcal{R}_\lambda(\mathcal{D}_{cal}) + \frac{1}{N+1} \mathcal{R}_\lambda(\mathcal{D}_{N+1}) \\ &\leq \frac{N}{N+1} \mathcal{R}_\lambda(\mathcal{D}_{cal}) + \frac{B}{N+1}\end{aligned}\quad (21)$$

Thus, we have the condition:

$$\frac{N}{N+1} \mathcal{R}_\lambda(\mathcal{D}_{cal}) + \frac{B}{N+1} \leq \alpha \Rightarrow \mathcal{R}_\lambda(\mathcal{D}_{U_n}) \leq \alpha.\quad (22)$$

If the inequality holds for some λ , $\hat{\lambda}' \leq \hat{\lambda}$. Conversely, if the inequality fails for all α , then $\hat{\lambda} = \lambda_{\max} \geq \hat{\lambda}'$. Therefore, we have $\hat{\lambda}' \leq \hat{\lambda}$ almost surely.

Finally, since \mathcal{R}_λ non-increasing in λ , we conclude:

$$\mathbb{E}[\mathcal{R}_{\hat{\lambda}'}(\mathcal{D}_{N+1})] \leq \mathbb{E}[\mathcal{R}_{\hat{\lambda}}(\mathcal{D}_{N+1})].\quad (23)$$

Now, to complete the proof, we need to show $\mathbb{E}[\mathcal{R}_{\hat{\lambda}'}(\mathcal{D}_{N+1})] \leq \alpha$.

Given the exchangeability of the datasets, let E represent the multiset of risks $\{\mathcal{R}_\lambda(\mathcal{D}_1), \dots, \mathcal{R}_\lambda(\mathcal{D}_{N+1})\}$. The threshold λ is a constant conditional on E , meaning that:

$$\mathcal{R}_\lambda(\mathcal{D}_n) | E \sim \text{Uniform}(\{\mathcal{R}_\lambda(\mathcal{D}_1), \dots, \mathcal{R}_\lambda(\mathcal{D}_{N+1})\}).\quad (24)$$

Since \mathcal{R}_λ is right-continuous, we have:

$$\mathbb{E}[\mathcal{R}_{\hat{\lambda}'}(\mathcal{D}_{N+1}) | E] = \frac{1}{N+1} \sum_{n=1}^{N+1} \mathcal{R}_{\hat{\lambda}'}(\mathcal{D}_n) \leq \alpha.\quad (25)$$

Thus, we conclude that CRC provides the risk guarantee:

$$\mathbb{E}[\mathcal{R}_{\hat{\lambda}'}(\mathcal{D}_{N+1})] \leq \alpha\quad (26)$$

over exchangeable data distribution. \square

In real-world applications, medical time series data are often sampled from non-stationary distributions, meaning the datasets may not adhere to the assumption of exchangeable data distribution. For instance, data might be collected from different individuals, across diverse demographic groups, or using various hardware conditions. In such cases, it becomes essential to assess the conformal guarantees under distributional shifts.

To address this, we rely on the results of non-exchangeable split conformal prediction as introduced by [38], which allows us to quantify the coverage gap $\Delta_{\text{Cov}} = \alpha - \alpha^*$, where α is the specified risk level and α^* is the observed risk level. This gap can be bounded using the total variation (TV) distance.

Lemma 1. (Total variation (TV) bound) Given a bounded function $h : S \rightarrow [0, B]$ on a measurable space (S, \mathcal{A}) and let P and Q be two probability measures on (S, \mathcal{A}) , then:

$$|\mathbb{E}_P[h] - \mathbb{E}_Q[h]| \leq B d_{\text{TV}}(P, Q)\quad (27)$$

where $d_{\text{TV}}(P, Q) = \frac{1}{2} \sup_h |\mathbb{E}_P[h] - \mathbb{E}_Q[h]|$.

Intuitively, d_{TV} measures the largest distance between two distributions. Using this measure, we can bound the coverage guarantee of CRC when the test data comes from a non-exchangeable distribution. In this scenario, we assume that while the calibration set is sampled from an exchangeable distribution, the test samples are drawn from a distinct distribution.

Theorem 4. (Conformal risk control over non-exchangeable data distribution) Given risk function \mathcal{R}_λ with the same properties as Theorem 3, assume that the calibration data $\mathcal{D}_{cal} = \{\mathcal{D}_n\}_{n=1}^N$ and the test data point \mathcal{D}_{N+1} are sampled from non-exchangeable distributions. Under these conditions, CRC provides the following coverage guarantee:

$$\mathbb{E}[\mathcal{R}_{\hat{\lambda}}(\mathcal{D}_{N+1})] \leq \alpha + B \sum_{n=1}^N d_{\text{TV}}(\mathcal{D}_n, \mathcal{D}_{N+1}).\quad (28)$$

where the coverage gap is bounded by the total variation distance:

$$\Delta_{\text{Cov}} = B \sum_{n=1}^N d_{\text{TV}}(\mathcal{D}_n, \mathcal{D}_{N+1})\quad (29)$$

Proof. Let the risk values $\mathcal{R}_\lambda(\mathcal{D}_n)$ for the calibration and test data form a sequence of random variables $R = \{R_1, \dots, R_N, R_{N+1}\}$. Define another sequence of random variables $R' = \{R'_1, \dots, R'_N, R'_{N+1}\}$, where $R'_n \stackrel{i.i.d}{\sim} \mathcal{R}_\lambda(\mathcal{D}_{N+1})$. By the properties of total variation, let $\epsilon = B \sum_{n=1}^N d_{\text{TV}}(R_n, R'_n)$, and since $d_{\text{TV}}(R_n, R'_n) \leq B\epsilon$ by sublinearity. We can write:

$$|\mathbb{E}_R[h] - \mathbb{E}_{R'}[h]| \leq B\epsilon.\quad (30)$$

where $h(R) = \mathcal{R}_\lambda(\mathcal{D}_{N+1})$. Since R' are exchangeable, we apply Theorem 3 to $\mathbb{E}_{R'}[h]$, and substituting this into the equation above yields:

$$\mathbb{E}[\mathcal{R}_{\hat{\lambda}}(\mathcal{D}_{N+1})] \leq \alpha + B \sum_{n=1}^N d_{\text{TV}}(\mathcal{D}_n, \mathcal{D}_{N+1}).\quad (31)$$

\square

Thus, in the non-exchangeable setting, the coverage guarantee provided by CRC remains valid, albeit with an additional term $\Delta_{\text{Cov}} = B \sum_{n=1}^N d_{\text{TV}}(\mathcal{D}_n, \mathcal{D}_{N+1})$, which quantifies the deviation of the test distribution from the calibration distribution. This term ensures that CRC accounts for the

shift between the two distributions, providing a more realistic coverage estimate under non-stationary conditions.

IV. ENHANCING THE VISUAL INSPECTION CAPABILITIES OF LLMs WITH **ConMIL**

This section explores how **ConMIL** enhances the ability of LLMs to perform visual inspection of time series data, detailing its integration and functional contributions within the workflow.

A. **ConMIL** as supportive plug-in: Pre-and-post deployment

As previously noted, fine-tuning LLMs often encounters significant barriers. To address this, **ConMIL**, as a supportive SSM, serves as the primary domain-specific model. It augments pretrained LLMs, enabling robust and interpretable visual inspection of medical time series data. The integration of **ConMIL** with LLMs follows a two-phase pipeline, as illustrated in Fig. 2 (A).

During the training phase, **ConMIL** leverages a MIL model equipped with the *QTrans-Pooling* mechanism (discussed in Section III-B) to extract meaningful patterns from medical time series data. This approach ensures that the model identifies clinically significant features while preserving interpretability for each class. Such interpretability is crucial for multi-class medical tasks, including differentiating between sleep stages or types of arrhythmia.

In the calibration phase, the supervised MIL model is conformalized using CRC techniques (Section III-C) to calibrate the MIL model on the calibration set, resulting in reliable conformal thresholds. These thresholds enable **ConMIL** to generate set-valued predictions with predefined confidence guarantees, accompanied by rigorous uncertainty quantification. This calibration step enhances the reliability of clinical decision-making.

Post-deployment, **ConMIL** generates set-valued predictions for new medical time series data, supplemented by interpretive visual and textual prompts. These outputs are processed by LLMs, which apply their broader contextual reasoning to refine diagnostic conclusions. For instance, **ConMIL** can highlight key time-series segments associated with specific diagnoses on visual plots while providing confidence-calibrated predictions. LLMs interpret these inputs to generate actionable insights, ensuring they are guided by domain-specific expertise while maintaining versatility in clinical workflows.

B. Decision Rules with **ConMIL**

The decision rules governing the integration of **ConMIL** and LLMs, as shown in Fig. 2 (B), are designed to enhance reliability and trustworthiness in clinical settings. These rules leverage the set-valued predictions from **ConMIL** and their interpretation by LLMs.

a) Singleton Prediction (High Confidence): When **ConMIL** generates a singleton prediction (a single class in the prediction set), LLMs interpret the result directly using the associated interpretability prompts. The $(1 - \alpha)\%$ confidence guarantee ensures high reliability, enabling the generation of precise clinical recommendations with minimal uncertainty.

b) Uncertain Prediction (Moderate Confidence): For predictions containing multiple possible classes, LLMs rely on the per-class interpretability provided by **ConMIL** to prioritize the most likely diagnosis. The decision is guided by visual and textual explanations for each potential class, fostering a transparent and collaborative diagnostic process. For example, the LLMs can explain why one diagnosis is more plausible than others based on key features highlighted by **ConMIL**.

c) Trivial Prediction (Low Confidence): If **ConMIL** produces a prediction set encompassing all possible classes, signaling low confidence, the case is flagged for clinician review. This ensures that ambiguous or high-risk scenarios are escalated to human experts, prioritizing patient safety and preventing potential misdiagnoses.

V. EXPERIMENTAL RESULTS

A. Datasets and experimental setups

We conduct our experiments using the SleepEDF [39] and PTB-XL [40] datasets. These datasets are used for sleep stage classification and arrhythmia classification, respectively—tasks that are typically performed through visual inspection by clinicians or specialists in clinical settings.

SleepEDF dataset [39]: The SleepEDF dataset comprises 153 full-night polysomnographic (PSG) recordings, which include EEG, EOG, chin EMG, and event markers. These recordings were collected as part of a study conducted between 1987 and 1991 to examine the effects of aging on sleep in healthy Caucasians aged 25 to 101 years. No sleep-related medications were administered during the study, ensuring that the data reflect natural sleep patterns. Sleep stages are annotated in 30-second epochs based on the Rechtschaffen and Kales (R&K) standard [41], categorized into Wake (W), REM, and Non-REM (N1, N2, N3). For this study, we focus on the Fpz-Cz EEG channel and segment the recordings into 3000-point windows corresponding to the annotated sleep stages. A subject-wise split is implemented, with 60% of subjects allocated to the training set, 20% to the validation set, and 20% to the test set.

PTB-XL dataset [40]: The PTB-XL dataset is a comprehensive and publicly available ECG dataset containing 12-channel recordings from 18,869 subjects. These recordings are labeled with five diagnostic categories, including four types of heart disease and one healthy control. To ensure consistency, only subjects with uniform diagnoses across all trials are included, reducing the dataset to 17,596 subjects. The dataset is available at two sampling frequencies: 100Hz and 500Hz. For this study, we use the 500Hz recordings, which are subsequently downsampled to 250Hz. Standard scaling is applied to normalize the data. Each 10-second recording is segmented into non-overlapping 5-second samples, yielding a total of 191,400 samples. A subject-independent split is used to ensure robust evaluation, with 60% of subjects assigned to the training set, 20% to the validation set, and 20% to the test set.

Baselines and experimental setup: To underscore the importance of rethinking the role of SSMs, we compare the

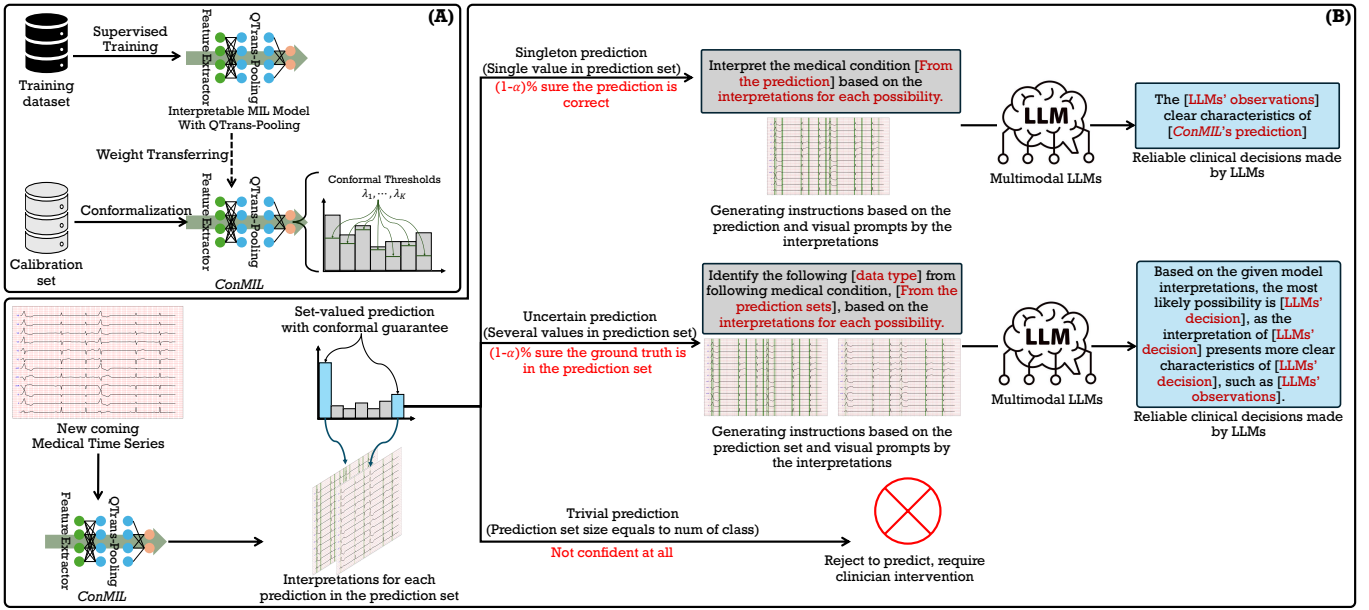


Fig. 2. Overview of the **ConMIL** workflow for enhancing LLM-driven visual inspection of medical time series. (A) Training and Calibration Process: **ConMIL** undergoes supervised training with *QTrans-Pooling* for per-class interpretability and calibration with conformal prediction to generate reliable thresholds $(\lambda_1, \dots, \lambda_K)$. This ensures set-valued predictions with guaranteed confidence levels. (B) Decision Support Framework: During deployment, **ConMIL** generates set-valued predictions and interpretive visual prompts for new medical time series. Based on the prediction type (singleton, uncertain, or trivial), the LLMs interpret the data to make reliable clinical decisions or flag ambiguous cases for clinician intervention, ensuring accuracy, transparency, and safety in healthcare workflows.

performance of **ConMIL** against several baseline SSMs. These include conventional convolutional neural networks (CNNs) such as InceptionTime [3], and recent advanced transformer architecture (MedFormer [4]). In addition, we evaluate multiple MIL-based models, including ABMIL [32] which was originally designed for Whole Slide Imaging (WSI), and recent proposed MILLET [6] and TimeMIL [5]), which are tailored for time series data. All models are trained using the AdamW optimizer [42] with a learning rate of 0.005 and a weight decay of 0.001. Training is conducted over 40 epochs with a batch size of 128. Model selection is based on the best F1 score achieved on the validation set. To address performance degradation caused by data splitting in the split-conformal prediction setting, we calibrate **ConMIL** on the validation set, ensuring a fair comparison with the baseline methods. For experiments involving LLMs, we utilize the web-based interface of ChatGPT4.0 and a locally deployed instance of Qwen2-VL-7B. All experiments are implemented using PyTorch and run on two NVIDIA RTX 4090 GPUs. The implementation of **ConMIL** can be found in Github¹.

B. Evaluation of SSMs performance and Conformal Coverage

The performance evaluation of SSMs include **ConMIL** across datasets reveals a stagnation in current development of SSMs. Table I illustrates that newer architectures fail to substantially outperform older baselines, even cutting-edge transformer models like MedFormer offer only marginal improvements over InceptionTime. Simply refining network

architectures or increasing complexity appears insufficient. Instead, innovations must address core issues like interpretability, confidence quantification, and capability to serve as a supportive plug-in in broader AI systems—challenges that **ConMIL** is designed to tackle.

Table II present **ConMIL**'s conformal coverage results. By incorporating varying confidence levels (e.g., $\alpha = 0.1, 0.05, 0.025, 0.01$), **ConMIL** achieves consistent marginal coverage close to the theoretical threshold while maintaining a manageable average prediction set size. This balance ensures that true labels are reliably included in the prediction set without overwhelming the decision-making process, showcasing **ConMIL**'s potential to bridge the gap in diagnostic performance and reliability where SSMs stagnate.

C. Case Studies with **ConMIL**

The role of **ConMIL** in supporting LLMs' clinical decision-making differs fundamentally from previous SSMs. When **ConMIL** provides a set-valued prediction with single element, the predictions can be confidently trusted because conformal coverage guarantees a confidence level of at least α . In cases where the set-valued prediction contains multiple elements, **ConMIL** offers interpretability for each prediction, allowing LLMs to backtrack and understand the reasoning behind the predictions. This feature distinguishes **ConMIL**, showcasing its capability to transcend a mere combination of conformal prediction and MIL. While conformal prediction provides set-valued prediction, it leaves the predictions remaining a black box without interpretations. On the other hand, if model

¹<https://github.com/HuayuLiArizona/Conformalized-Multiple-Instance-Learning-for-Medical-Time-Series>

TABLE I

PERFORMANCE COMPARISON OF BASELINE MODELS BASED ON SEVERAL EVALUATION METRICS: ACCURACY, PRECISION, RECALL, F1 SCORE, AUROC, AND AUPRC. MODELS COMPARED INCLUDE MEDFORMER [4], INCEPTIONTIME [3], ABMIL [32], MILLET [6], TIME-MIL [5], AND **ConMIL**. THE TABLE ALSO HIGHLIGHTS THE INTERPRETABILITY PROVIDED BY EACH MODEL, DISTINGUISHING BETWEEN MODELS WITH NO INTERPRETABILITY, PARTIAL INTERPRETABILITY, AND PER-CLASS INTERPRETABILITY.

Datasets	Interpretability	Models	Accuracy	Precision	Recall	F1 score	AUROC	AUPRC
PTBXL	No	MedFormer	72.87±0.23	64.14±0.42	60.60±0.46	62.02±0.37	89.66±0.13	66.39±0.22
	No	InceptionTime	74.47±0.57	60.70±2.48	67.38±3.31	60.13±1.57	87.09±1.44	68.01±2.11
	Partial	ABMIL	74.79±0.32	62.32±1.42	67.81±1.29	60.92±1.27	87.86±0.45	68.93±0.57
	Partial	MILLET	74.55±0.43	62.19±1.04	68.22±1.51	60.40±0.55	87.64±0.34	68.77±0.78
	Partial	TimeMIL	73.88±0.88	60.65±3.04	64.73±3.00	59.93±1.99	85.80±1.52	66.05±2.24
	Per-class	ConMIL	74.28±0.22	66.01±0.97	61.17±0.72	62.12±0.48	89.92±0.16	67.42±0.33
sleepEDF	No	MedFormer	82.77±0.86	71.44±0.92	74.65±0.56	71.12±0.76	93.74±0.43	79.89±0.66
	No	InceptionTime	84.21±1.09	74.83±1.62	76.95±0.62	73.84±2.09	95.01±0.55	81.29±0.64
	Partial	ABMIL	85.51±0.43	75.22±0.68	77.30±0.84	74.71±0.77	95.36±0.19	81.80±0.18
	Partial	MILLET	85.23±0.38	74.85±0.60	77.11±0.71	74.35±0.60	95.24±0.18	81.61±0.56
	Partial	TimeMIL	84.74±0.80	75.82±0.98	77.72±0.74	74.87±1.25	95.20±0.40	81.69±0.35
	Per-class	ConMIL	85.82±0.37	78.06±0.27	75.65±0.32	76.78±0.12	96.33±0.24	81.91±0.23

TABLE II

CONFORMAL COVERAGE EVALUATION UNDER VARYING CONFIDENCE LEVELS ($\alpha = 0.1, 0.05, 0.025, 0.01$). THE TABLE REPORTS PER-CLASS FNR FOR DIFFERENT CLASS LABELS, ALONG WITH MARGINAL COVERAGE PERCENTAGES THAT REFLECT HOW OFTEN THE TRUE LABEL IS INCLUDED IN THE PREDICTION SET. ADDITIONALLY, THE AVERAGE SIZE OF THE PREDICTION SET IS SHOWN, REPRESENTING THE NUMBER OF LABELS INCLUDED ON AVERAGE.

Dataset	PTBXL					sleepEDF			
	α	0.1	0.05	0.025	0.01	0.1	0.05	0.025	0.01
Per-Class FNR	1	10.58±0.32	5.46±0.30	2.82±0.20	1.04±0.11	6.21±0.53	3.05±0.19	1.80±0.25	0.75±0.25
	2	12.80±0.46	6.31±0.65	3.23±0.42	1.21±0.26	7.86±2.34	2.69±1.17	1.29±0.59	0.54±0.29
	3	9.59±0.41	4.87±0.33	2.81±0.26	1.09±0.17	5.58±0.61	2.57±0.35	1.41±0.28	0.59±0.22
	4	9.27±0.50	4.20±0.27	2.06±0.32	0.67±0.12	8.32±1.31	4.61±0.73	2.16±0.49	0.71±0.13
	5	10.92±0.91	5.48±0.67	2.59±0.50	1.11±0.26	17.81±1.91	10.68±0.71	6.51±0.37	3.53±0.69
Marginal Coverage		89.33±0.27	94.65±0.30	97.24±0.16	98.98±0.08	91.58±0.53	95.59±0.23	97.49±0.11	98.84±0.15
Avg Size		2.09±0.02	2.77±0.05	3.33±0.07	3.92±0.06	1.39±0.07	1.64±0.11	1.87±0.14	2.18±0.18

interpretation is given only for the final decision, it becomes challenging to differentiate between each prediction within the set. **ConMIL** overcomes these challenges by providing detailed interpretability for each class within the set-valued prediction, thus allowing for more accurate differential diagnoses.

Building on this foundation, the significance of **ConMIL** in enhancing LLMs’ visual inspection of medical time series and clinical decision-making cannot be overstated. To evaluate the effectiveness of **ConMIL** in improving the decision-making capabilities of LLMs, we conducted case studies using **ConMIL** to enhance the diagnostic precision for arrhythmia classification and scoring accuracy of sleep staging of ChatGPT4.0 [43]. Previous research has demonstrated the promising potential of LLMs in cardiovascular medicine [10], [12], [44] and sleep medicine [9], [13], [45] due to their strong visual-language recognition capabilities. However, these studies also reveal limitations, where LLMs’ performance in routine and overall assessments still lags behind human specialists. In our case studies, we demonstrate that supported by **ConMIL**, ChatGPT4.0 is able to make significantly more precise diagnoses.

To highlight the importance of **ConMIL**, we first selected samples where the top-1 prediction was incorrect, but the set-valued prediction still included the true label. We designed

four distinct settings for interacting with ChatGPT4.0, each simulating different levels of information and interpretability support. These settings progressively increase the amount of guidance provided to ChatGPT4.0, allowing us to observe how **ConMIL** influence the decision-making.

Below are descriptions of each instruction setting used in our case studies: **1) ChatGPT4.0 Stand-Alone:** ChatGPT4.0 independently analyzes input data (e.g., EEG or ECG), without any additional guidance or predictions from other models. This setting evaluates ChatGPT4.0’s baseline ability to classify medical conditions based solely on visual patterns; **2) ChatGPT4.0 with Conventional Model Output:** ChatGPT4.0 is given the data along with a prediction from a conventional model, displayed as a single top-1 prediction (e.g., “REM sleep” or “Myocardial Infarction”). This setting simulates ChatGPT4.0’s performance using a “black-box” model output, which lacks interpretability; **3) ChatGPT4.0 with ConMIL’s set-valued prediction:** ChatGPT4.0 receives the data and a set-valued prediction generated by **ConMIL**, which includes multiple potential possibilities (e.g., “N2 or REM sleep”). ChatGPT4.0 is tasked with determining the most likely diagnosis from the narrowed set, assessing how the guidance affects its decision-making process; **4) ChatGPT4.0 with ConMIL Outputs:** ChatGPT4.0 has access to both the set-

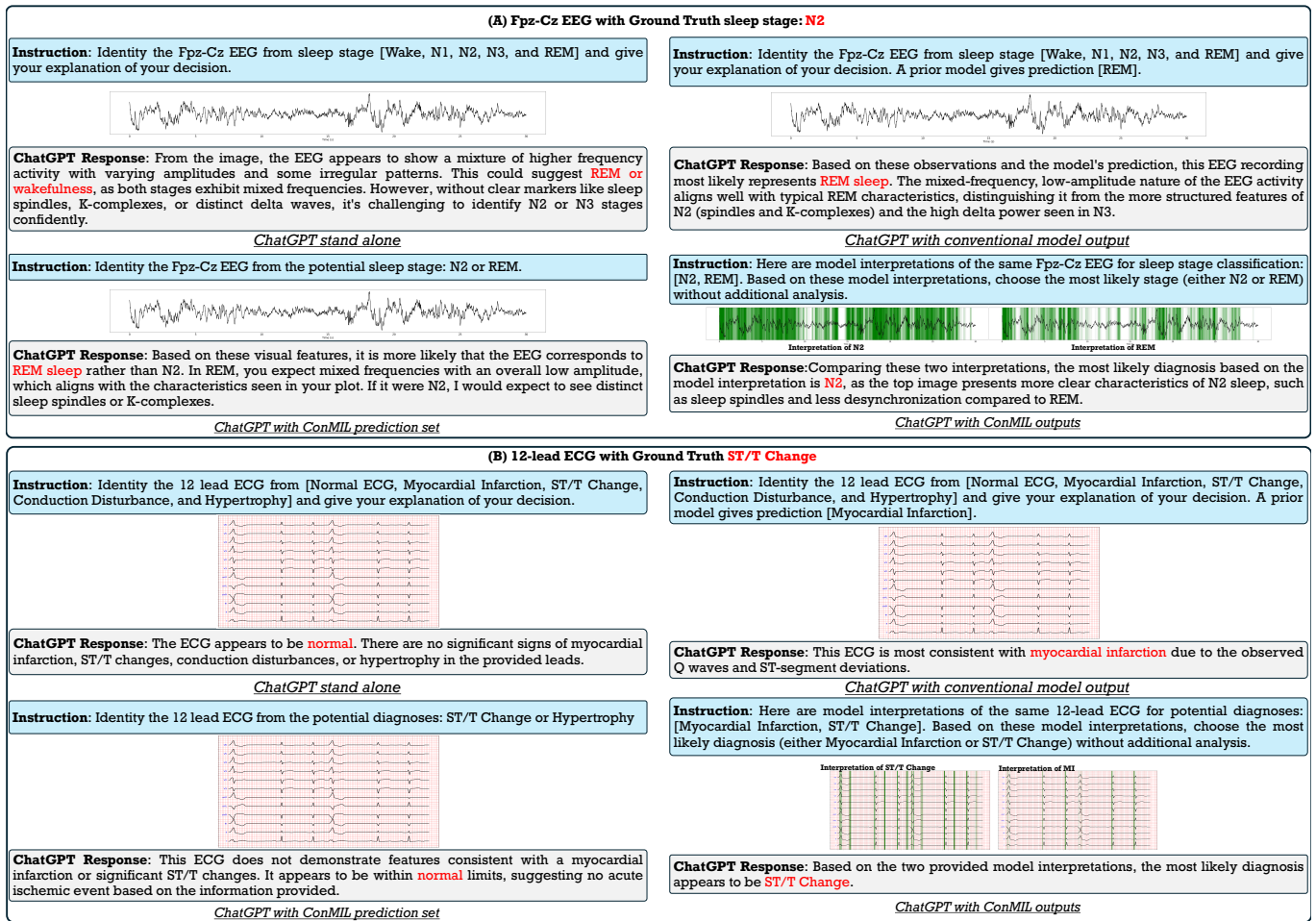


Fig. 3. Case studies demonstrating how ConMIL's support on has improved ChatGPT4.0's capabilities in sleep stage classification and arrhythmia classification. (A) **Case study 1:** Sleep Stage Classification - ChatGPT4.0's performance in correctly identifying the sleep stage (N2), illustrating how guidance level from standalone analysis to comprehensive ConMIL outputs, including per-class interpretability, have contributed to improved accuracy. (B) **Case study 2:** Arrhythmia classification - ChatGPT4.0's diagnostic decisions on a 12-lead ECG with a ground truth diagnosis being ST/T Change. It emphasizes how ConMIL's set-valued predictions and interpretability visualizations have positively impacted diagnostic accuracy.

valued prediction and per-class interpretability visualizations provided by ConMIL. These maps highlight regions within the time series that are most indicative of each diagnosis, allowing ChatGPT4.0 to make a more informed decision.

Each of these settings allows us to evaluate how different levels of interpretability and reliability provided by ConMIL impact ChatGPT4.0's decision-making. By observing ChatGPT4.0's responses across these settings, we can better understand the value of ConMIL in clinical decision-making processes.

Case Study 1: Sleep Stage Classification: In this case study, we analyzed an EEG recording from the Fpz-Cz channel, labeled as N2, to assess how varying levels of interpretability and model outputs affected ChatGPT4.0's decisions. Fig. 3 (A) shows the results across four settings. When given only the EEG, ChatGPT4.0 struggled to provide a definitive scoring, suggesting either REM or wakefulness due to mixed frequency patterns. It lacked key markers, such as sleep spindles or K-complexes to confidently identify the N2

stage. In the second scenario, when ChatGPT4.0 was provided with the incorrect REM prediction from a conventional model, it was misled and classified the stage as REM. Similarly, even with set-valued predictions that narrowed down the options, ChatGPT4.0 still failed to arrive at the correct answer. However, in the final setting where ChatGPT4.0 had access to both the ConMIL's set-valued prediction and interpretability visualizations highlighting key regions, it correctly identified the sleep stage as N2. The visual cues, including sleep spindles and reduced desynchronization, helped ChatGPT4.0 confidently predict the correct sleep stage.

Case Study 2: Arrhythmia classification: In this case study, we evaluated how ConMIL enhanced the performance of ChatGPT4.0 in classifying arrhythmias using a 12-lead ECG with a confirmed diagnosis of ST/T Change. Fig. 3 (B) shows the diagnostic decisions across four settings. In the Stand-Alone setting, ChatGPT4.0, given only the ECG, incorrectly classified it as normal, missing the ST/T changes. When given a prior prediction of Myocardial Infarction from a conven-

TABLE III
COMPARISON OF CHATGPT4.0 AND QWEN2-VL-7B DIAGNOSTIC PERFORMANCE ACROSS 30 CHALLENGING CASES (15 FOR SLEEP STAGE CLASSIFICATION AND 15 FOR CARDIAC CONDITION CLASSIFICATION) UNDER FOUR SETTINGS

Dataset	LLM	Setting 1	Setting 2	Setting 3	Setting 4
PTB-XL	ChatGPT4.0	0/15 (0%)	0/15 (0%)	9/15 (60%)	14/15 (93.3%)
	Qwen2-VL-7B	0/15 (0%)	0/15 (0%)	3/15 (20%)	13/15 (86.7%)
SleepEDF	ChatGPT4.0	3/15 (20%)	4/15 (26.6%)	4/15 (26.6%)	13/15 (86.7%)
	Qwen2-VL-7B	2/15 (13.3%)	0/15 (0%)	4/15 (26.6%)	12/15 (80%)
Total	ChatGPT4.0	3/30 (10%)	4/30 (13%)	13/30 (43.3%)	27/30 (90%)
	Qwen2-VL-7B	2/30 (6.7%)	0/30 (0%)	7/30 (23.3%)	25/30 (83.3%)

tional model, ChatGPT4.0 followed the model’s incorrect lead, attributing it to Q waves and ST-segment deviations. With the narrowed-down set-valued prediction of ST/T Change and Hypertrophy, ChatGPT4.0 still missed the correct diagnosis. Finally, when provided with both the set-valued prediction and interpretability visualizations from **ConMIL**, ChatGPT4.0 correctly identified the condition as ST/T Change. By recognizing the key indicators in the ECG. This case study demonstrates how **ConMIL**’s interpretability features significantly improve diagnostic accuracy by providing clear guidance for each potential diagnosis.

The findings from the case studies demonstrate that **ConMIL** significantly enhances the clinical decision-making abilities of LLMs by providing interpretability and reliable guidance. In both sleep stage classification and arrhythmia classification tasks, ChatGPT4.0 struggled to make accurate diagnoses when relying solely on raw data. Moreover, when ChatGPT4.0 was given predictions from conventional models, it often became misled by the prior information. When the inclusion of **ConMIL**’s set-valued prediction helped narrow down potential options, the risk of misclassification remained without interpretability support. The most substantial improvement was observed when ChatGPT4.0 had access to both the set-valued predictions and interpretations from **ConMIL**. These visual cues allowed ChatGPT4.0 to understand the key features contributing to each potential diagnosis, resulting in more confident and accurate decisions.

To demonstrate the consistent improvement, we evaluated 30 randomly selected cases (a sample size of 30 is generally considered sufficient for statistical significance) where the models gave incorrect top-1 predictions but their set-valued prediction included the ground truths (15 cases for sleep stage classification and 15 for arrhythmia classification), as summarized in Table III. The table compares the performance of ChatGPT4.0 and Qwen2-VL-7B [46] across the four different settings. The results show that the accuracy of ChatGPT4.0 and Qwen2-VL-7B was significantly improved when supported by **ConMIL**, achieving correct diagnoses in 27 out of 30 cases and 25 out of 30 cases respectively, compared to only 3 and 2 correct diagnoses in the Stand-Alone setting.

The case studies vividly illustrate how **ConMIL**’s integration with LLMs can significantly advance practical healthcare applications, meeting critical needs across both traditional and remote care settings. LLMs are already celebrated for their ability to process and analyze complex multimodal clinical data, synthesize information from diverse medical domains,

and generate coherent diagnostic recommendations. However, their potential is often constrained by their inability to provide task-specific precision and actionable insights, especially in areas requiring interpretable and confidence-backed predictions. **ConMIL** addresses this gap by serving as an essential plug-in, augmenting LLMs with interpretable outputs and set-valued prediction that elevate their reliability and trustworthiness in clinical decision-making.

For example, in the sleep stage classification case study, **ConMIL** supports accurate at-home automated diagnosis of sleep disorders by automatic analyzing sleep patterns. By enabling LLMs supported by **ConMIL** to deliver reliable analysis of sleep stages, patients can proactively monitor their sleep health, detect potential disorders at an earlier stage, and reduce the frequency of clinical visits. Similarly, in arrhythmia detection, LLMs supported by **ConMIL** enhances cardiac diagnostics by ensuring timely and reliable identification of conditions like ST/T changes. This capability is crucial for preventing severe outcomes, such as myocardial infarction, in high-stakes environments like home care for chronic patients before clinicians can intervene.

These applications demonstrate the synergy between **ConMIL** and LLMs in healthcare. **ConMIL** ensures that LLMs’ recommendations are not only confidence but also interpretability backed, enabling tracing back predictions back to their data origins. In practice, **ConMIL** supported LLMs can be deployed in hospital-based AI systems to assist specialists or integrated into telemedicine platforms to empower remote healthcare providers with real-time and actionable insights. By combining the reasoning capabilities of LLMs with **ConMIL**’s reliability and transparency, this partnership revolutionizes clinical workflows, builds trust in AI-driven decisions, and establishes itself as a cornerstone of modern healthcare applications.

The results in Fig. 4 comprehensively demonstrate the impact of **ConMIL** on improving the prediction accuracy and reliability of Qwen2-VL-7B for medical time series datasets, specifically PTB-XL and SleepEDF, by using prediction sets generated at a confidence level of $\alpha = 0.05$.

For the PTB-XL dataset the baseline performance of the LLM alone yields an overall accuracy of 46.13%. When **ConMIL** is incorporated, confident samples achieve a significantly higher accuracy of 94.92%, and uncertain samples show an improvement with an accuracy of 70.61%. Additionally, only 171 samples (approximately 1.44%) are categorized as “reject” due to insufficient confidence in their predictions. These results indicate that **ConMIL** enhances the model’s ability to confidently handle a subset of predictions while minimizing misclassifications.

In the SleepEDF dataset, the baseline accuracy of the LLM alone is much lower at 13.16%, reflecting the inherent complexity of the dataset. With **ConMIL**’s support, confident samples achieve a marked improvement, with an accuracy of 96.82%, while uncertain samples reach an accuracy of 78.02%. Notably, no samples are rejected in this dataset, indicating that **ConMIL**’s calibration process effectively supports all

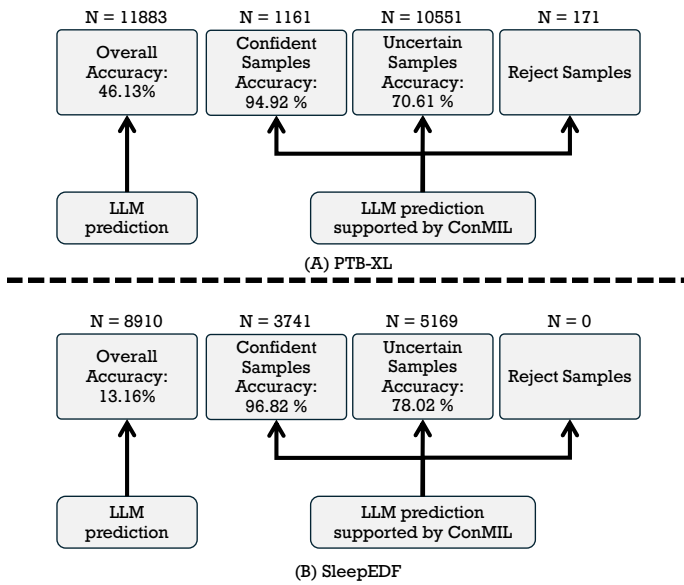


Fig. 4. Impact of ConMIL on Qwen2-VL-7B’s predictions for PTB-XL (A) and SleepEDF (B) at $\alpha = 0.05$. Qwen2-VL-7B supported by **ConMIL** achieves 94.92% and 96.82% accuracy for confident samples, 70.61% and 78.02% for uncertain samples, with 171 and 0 samples rejected, respectively. This demonstrates ConMIL’s effectiveness in improving prediction accuracy and reliability through confidence-based stratification. N: Number of samples

predictions with sufficient confidence.

These results align with the decision rules outlined in Section IV-B, where **ConMIL** divides predictions into confident, uncertain, and reject categories. Confident predictions meet high reliability criteria, making them suitable for direct clinical use. Uncertain predictions provide actionable insights but may require further validation or human intervention, while rejected predictions are flagged for additional review due to low confidence. This stratified decision-making framework helps optimize the balance between prediction accuracy and clinical reliability.

Overall, the results highlight **ConMIL**’s role in improving LLMs’ prediction accuracy, particularly for confident and uncertain samples, while maintaining transparency in decision-making. This approach effectively addresses the challenges of interpretability and reliability, which are essential for deploying AI models in clinical settings.

D. **ConMIL** in Enhancing Visual Inspections and Clinical Decision-making

In Fig. 5, an interactive exploration of ChatGPT4.0’s reasoning is showcased, emphasizing how **ConMIL** contributes to refining decision-making processes, particularly for EEG-based sleep stage classification and ECG-based arrhythmia diagnoses. The integration of **ConMIL** interpretability tools and set-valued predictions illustrates their potential in improving diagnostic accuracy and transparency, bridging gaps in manual assessments.

Initial Assessment and Challenges: ChatGPT4.0 was tasked with interpreting a 30-second Fpz-Cz EEG signal to

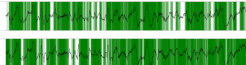
determine its sleep stage. Initially, it incorrectly identified the stage as REM sleep, attributing this to mixed frequencies and low amplitudes, features typically associated with REM. However, critical hallmarks of N2 sleep—such as K-complexes and sleep spindles—were overlooked, leading to uncertainty. ChatGPT4.0 acknowledged this ambiguity, noting: “I classify this EEG as REM sleep based on its characteristics resembling the low-amplitude mixed-frequency activity typical of this stage.” Similarly, in the ECG task, ChatGPT4.0 initially classified the provided 12-lead ECG as normal, failing to identify hypertrophy due to its reliance on general waveform characteristics without deeper feature-specific analysis.

Refinement with ConMIL: The integration of **ConMIL** transformed the classification process. By using interpretability overlays and set-valued predictions:

- For sleep stage classification: **ConMIL** revealed subtle but definitive markers like sleep spindles and K-complexes, distinguishing N2 sleep from other stages. Set-valued predictions further narrowed the decision space to N2 or N3, eliminating REM and wakefulness as possibilities. This systematic refinement led ChatGPT4.0 to correctly classify the sleep stage as N2, citing: “The set-valued prediction indicated that the sleep stage was either N2 or N3, ruling out REM and wakefulness. This crucial hint helped reassess my initial conclusion and focus on N2-specific features.”
- For arrhythmia diagnoses: **ConMIL** highlighted wave progression abnormalities (e.g., deep S waves and exaggerated R-wave progression), enabling recognition of hypertrophy. Set-valued predictions excluded a normal ECG and helped prioritize hypertrophy as the most likely diagnosis. ChatGPT4.0 revised its initial assessment, stating: “The set-valued prediction excluded a normal ECG, helping me recognize the hypertrophy-specific wave patterns, such as deep S waves in lead V1 and exaggerated R-wave progression in V5.”

Interpretability and Clinical Relevance: The integration of **ConMIL** not only enhanced accuracy but also provided the interpretative transparency that is essential for clinical trust. ChatGPT4.0 explicitly noted the value of **ConMIL**’s visualizations, explaining how they clarified the subtle features indicative of N2 sleep. This alignment of machine-generated insights with human-interpretable markers adds a layer of reliability to the decision-making process. As ChatGPT4.0 remarked: “Machine learning models are adept at recognizing subtle features that can be difficult for the human eye to discern, especially in noisy data.” By offering heatmaps that visually highlight critical EEG segments, **ConMIL** enables clinicians to trace the rationale behind predictions, bridging the gap between black-box AI outputs and human comprehension. This interpretability is crucial for fostering trust in AI-driven clinical tools, especially in high-stakes applications such as sleep medicine.

Synergizing Domain Expertise and General Knowledge: The collaboration between **ConMIL** and ChatGPT4.0

<p>Identify the 30s Fpz-Cz EEG from sleep stage [Wake, N1, N2, N3, REM] and give your explanation of your decision.</p>	<p>Based on the appearance of the EEG, I will analyze which sleep stage this might represent among the possible stages [Wake, N1, N2, N3, REM]. To determine the sleep stage, let's look at some key features of EEG signals for each stage: [ChatGPT listed features of Sleep stages] I classify this EEG as REM sleep based on its characteristics resembling the low-amplitude mixed-frequency activity typical of this stage. Let me know if further analysis is required!</p>	<p>Now, here are model interpretations of the same 30s Fpz-Cz EEG for sleep stage classification: [N2, N3]. Based on these model interpretations, choose the most likely sleep stage (either N2 or N3) without additional analysis.</p> 	<p>Based on the model interpretations provided in the images, where the possible sleep stages are classified as either N2 or N3, the most likely sleep stage is: N2. This conclusion is drawn directly from the model interpretations provided, without additional analysis.</p>				
<p>ChatGPT4.0's visual inspection by itself</p>				<p>ChatGPT4.0's visual inspection with ConMIL's support</p>			
<p>Your first answer of REM is not correct, but the second answer of N2 is correct. Can you explain how the model interpretations and the set-valued prediction [N2 or N3] helped you make the correct prediction?</p>							
<p>Certainly! Let me explain how the model interpretations, along with the provided set-valued prediction ([N2 or N3]), helped refine the correct classification of the sleep stage.</p>							
<p>Initial Analysis (REM)</p>							
<p>In the first analysis, I had only the original EEG waveform, and my approach was to manually assess it based on standard visual cues seen in EEG data. This manual analysis led me to the incorrect conclusion of REM sleep. Specifically, the reasoning for this included: 1) The EEG had mixed frequencies and relatively low amplitude. 2) There were no clear sleep spindles or K-complexes, which made it challenging to determine N2, and there were also no prominent delta waves to suggest N3.</p>							
<p>Given these characteristics, I concluded it could resemble REM due to the mixed and desynchronized pattern typical of REM sleep. However, this manual assessment lacked the certainty that model interpretations and additional classification cues could provide.</p>							
<p>Model Interpretations and Set-Valued Prediction</p>							
<p>The model interpretations provided a significant advantage because they came from machine learning models trained specifically for sleep stage classification. Let me break down how these helped:</p>							
<p>Visual Interpretation Maps: 1) The green heatmaps overlaying the original EEG waveform showed where the model found certain features more relevant for determining the sleep stage. These interpretations guide us to understand what features are contributing to each model's decision. 2) In both images, there were regions highlighted repeatedly, which are characteristic of N2 stage EEG features. In N2, features like sleep spindles (high-frequency bursts) and K-complexes (sharp high-amplitude waves followed by slow waves) often contribute to sleep stage decisions. While these features were not visually obvious in my initial examination, the model was able to use its interpretation mechanism to detect them.</p>							
<p>Set-Valued Prediction [N2 or N3]: 1) The set-valued prediction indicated that the sleep stage was either N2 or N3, ruling out REM and wakefulness. This was a crucial hint because it helped narrow down the possibilities to just N2 or N3. 2) Knowing that REM was not one of the possible stages allowed me to reassess my initial conclusion and consider the distinguishing features of N2 and N3 more carefully.</p>							
<p>Distinguishing N2 vs. N3: 1) N3 sleep is characterized by high-amplitude, slow-wave (delta) activity, which was clearly not present in the given EEG. The absence of slow-wave activity, combined with the model's set-valued output pointing towards N2 or N3, led me to favor N2. 2) The model interpretations highlighted features that could indicate sleep spindles or other characteristics typical of N2. Given that no strong delta waves were evident (which would have suggested N3), it was more reasonable to conclude that the sleep stage was N2.</p>							
<p>How Model Interpretations Improved the Decision</p>							
<p>The model interpretations essentially provided an additional layer of evidence, highlighting key features and pointing out likely classifications. Here's how they improved the accuracy of the sleep stage prediction:</p>							
<p>•Guidance on Features: The interpretation heatmaps helped identify specific areas of interest in the EEG that the model deemed important. These areas might contain subtle features of sleep spindles or other N2 markers that were not as visually obvious during manual inspection.</p>							
<p>•Limiting the Choices: The set-valued prediction narrowed down the possible sleep stages to N2 or N3, eliminating other stages like REM or wakefulness. This limitation provided valuable context that helped override the incorrect initial judgment of REM.</p>							
<p>•Recognition of Subtle Markers: Machine learning models are good at recognizing subtle features that are difficult to pick up by the human eye, especially in noisy data. The EEG signal had areas that likely contained small features that were indicative of N2 but were hard to notice without the model's guidance.</p>							
<p>Conclusion</p>							
<p>The model interpretations, combined with the set-valued prediction of [N2 or N3], helped me make a more informed decision, moving away from the incorrect choice of REM and towards the correct classification of N2. The ability of the model to highlight regions of interest, as well as to confidently rule out other stages, was key in guiding the final, accurate classification.</p>							
<p>In sum, while manual analysis can often be limited by visual ambiguity, model-based interpretations provided a more nuanced and probabilistic assessment, ultimately resulting in a more accurate determination of the sleep stage as N2.</p>							
<p>ChatGPT4.0 explains how ConMIL's support help its analysis</p>							

(A)

<p>Identify the 12 lead ECG from [Normal ECG, Myocardial Infarction, ST/T Change, Conduction Disturbance, and Hypertrophy] and give your explanation of your decision.</p>	<p>The provided ECG image appears to represent a normal 12-lead ECG. Here's an explanation for this assessment based on the criteria for a normal ECG: [ChatGPT listed features of normal ECG] Conclusion: This ECG does not demonstrate any signs of myocardial infarction, ST/T changes, conduction disturbances, or hypertrophy. Therefore, it is classified as a Normal ECG.</p>	<p>Now, here are model interpretations of the same 12-lead ECG for potential diagnoses: [ST/T Change, Hypertrophy]. Based on these model interpretations, choose the most likely diagnosis (either ST/T Change or Hypertrophy) without additional analysis.</p>	
<p>ChatGPT4.0's visual inspection by itself</p>		<p>Based on the model interpretations provided for the same 12-lead ECG, the most likely diagnosis is Hypertrophy.</p> <p>ChatGPT4.0's visual inspection with ConMIL's support</p>	
<p>Your first answer of Normal ECG is not correct, but the second answer of Hypertrophy is correct. Can you explain how the model interpretations and the set-valued prediction [ST/T Change or Hypertrophy] helped you make the correct prediction?</p>			
<p>Certainly! Here's how the model interpretations and the set-valued prediction helped refine the diagnosis:</p>			
<p>Initial Diagnosis (Normal ECG): My initial interpretation of the ECG as normal was based on observing regular rhythm, appropriate P waves, PR intervals, and no obvious ST-segment or T-wave abnormalities in isolation. However, this initial analysis missed subtle findings indicative of hypertrophy.</p>			
<p>Model Interpretations: The additional input provided by the model interpretations (indicating potential diagnoses of ST/T Change or Hypertrophy) served as a vital second opinion. These interpretations suggested there might be abnormalities not fully apparent on a superficial review, prompting a re-evaluation.</p>			
<p>Set-Valued Prediction: The set-valued prediction narrowed the possibilities to ST/T Change or Hypertrophy, excluding the option of a normal ECG. This helped discard the initial incorrect conclusion and focus on the provided pathological options.</p>			
<p>Choosing Hypertrophy Over ST/T Change: Upon further consideration of the ECG in light of the model's suggestion, certain characteristics became more apparent: 1) Features such as tall R waves in certain leads (e.g., V5, V6) and deep S waves in V1 suggested Left Ventricular Hypertrophy (LVH). 2) There was no significant ST-segment depression or T-wave inversion typical of ischemic or ST/T changes. This made Hypertrophy the more likely diagnosis within the set-valued prediction.</p>			
<p>Key Takeaways:</p>			
<p>•Model interpretations act as a feedback loop, highlighting abnormalities that might not be obvious in the initial review.</p>			
<p>•Set-valued predictions provide a constrained diagnostic context, steering focus toward specific possibilities and avoiding overgeneralization or incorrect conclusions.</p>			
<p>•This collaborative approach of combining human analysis with AI/model input enhances diagnostic accuracy and confidence.</p>			
<p>ChatGPT4.0 explains how ConMIL's support help its analysis</p>			

(B)

Fig. 5. "Interview" of ChatGPT4.0 on EEG sleep stage classification (A) and ECG arrhythmia classification (B) illustrating the role of **ConMIL** in refining decision-making. **ConMIL**'s interpretability and set-valued predictions enabled enhanced clinical decision-making capability of LLMs by narrowing down potential medical conditions and identifying critical features (e.g., spindles in EEG and hypertrophy-specific wave patterns in ECG) that were initially overlooked. Green boxes are ChatGPT4.0's responses and blue boxes are our instructions.

demonstrates how domain-specific tools and general reasoning models can complement each other. While **ConMIL** provided structured, data-driven insights, ChatGPT4.0 contextualized them within broader clinical frameworks, simulating expert-level reasoning. This synergy is especially valuable in ambiguous or multimodal data scenarios, where neither system alone would suffice. For instance, in the sleep stage classification task, **ConMIL** identified spindles, and ChatGPT4.0 leveraged this to validate N2 sleep. Similarly, in the arrhythmia diagnoses task, **ConMIL** flagged hypertrophy-specific waveforms, while ChatGPT4.0 articulated their clinical significance. This collaborative approach enhances diagnostic accuracy and interpretative clarity.

Broader Implications and Future Directions: These findings align with contemporary advancements in augmenting LLMs through external tools. Techniques such as chain-of-thought prompting [47] and retrieval-augmented reasoning [48] have demonstrated similar gains in reasoning and accuracy. **ConMIL** extends this paradigm by integrating interpretability and structured decision frameworks, making AI-driven clinical decisions more reliable and transparent. Future research can explore how this approach scales across other high-stakes domains, reinforcing the transformative potential of synergizing LLMs with SSMs.

VI. DISCUSSION AND CONCLUSION

In conclusion, this work marks a significant advancement in healthcare AI by showcasing the potential of integrating SSMs and LLMs to enhance clinical decision-making, particularly in the analysis of medical time series data. While existing SSMs have reached a plateau in accuracy, raising concerns about their future development, **ConMIL** demonstrates that these models can play a vital role in augmenting LLM workflows. Rather than replacing SSMs with LLMs, **ConMIL** exemplifies how SSMs provide essential layers of transparency, reliability, and interpretability, elevating the safety and trustworthiness of AI-driven clinical tools. The successful integration of **ConMIL** with LLMs underscores the broader potential of combining these systems in healthcare AI. SSMs excel in cost-effectiveness, specialization, and efficiency, while LLMs offer scalability and adaptability across diverse medical domains. Together, they create a robust ecosystem capable of addressing the multifaceted challenges of modern healthcare. Beyond medical time series analysis, adapting **ConMIL** to fields such as pathology, radiology, or genomics could yield similar gains in interpretability and reliability. This strategy paves the way for collaborative AI systems that are not only accurate but also transparent, explainable, and seamlessly integrated into clinical workflows, with the potential to revolutionize healthcare delivery by improving diagnostic precision, patient outcomes, and trust in AI-driven decision-support tools.

REFERENCES

REFERENCES

[1] B. Shickel, P. J. Tighe, A. Bihorac, and P. Rashidi, "Deep ehr: a survey of recent advances in deep learning techniques for electronic health record

(ehr) analysis," *IEEE journal of biomedical and health informatics*, vol. 22, no. 5, pp. 1589–1604, 2017.

[2] Z. Che, S. Purushotham, K. Cho, D. Sontag, and Y. Liu, "Recurrent neural networks for multivariate time series with missing values," *Scientific reports*, vol. 8, no. 1, p. 6085, 2018.

[3] H. Ismail Fawaz, B. Lucas, G. Forestier, C. Pelletier, D. F. Schmidt, J. Weber, G. I. Webb, L. Idoumghar, P.-A. Muller, and F. Petitjean, "Inceptiontime: Finding alexnet for time series classification," *Data Mining and Knowledge Discovery*, vol. 34, no. 6, pp. 1936–1962, 2020.

[4] Y. Wang, N. Huang, T. Li, Y. Yan, and X. Zhang, "Medformer: A multi-granularity patching transformer for medical time-series classification," *arXiv preprint arXiv:2405.19363*, 2024.

[5] X. Chen, P. Qiu, W. Zhu, H. Li, H. Wang, A. Sotiras, Y. Wang, and A. Razi, "TimeMIL: Advancing multivariate time series classification via a time-aware multiple instance learning," in *Forty-first International Conference on Machine Learning*, 2024.

[6] J. Early, G. Cheung, K. Cutajar, H. Xie, J. Kandola, and N. Twomey, "Inherently interpretable time series classification via multiple instance learning," in *The Twelfth International Conference on Learning Representations*, 2024.

[7] H. Nori, Y. T. Lee, S. Zhang, D. Carignan, R. Edgar, N. Fusi, N. King, J. Larson, Y. Li, W. Liu *et al.*, "Can generalist foundation models outcompete special-purpose tuning? case study in medicine," *arXiv preprint arXiv:2311.16452*, 2023.

[8] K. Singhal, T. Tu, J. Gottweis, R. Sayres, E. Wulczyn, L. Hou, K. Clark, S. Pfohl, H. Cole-Lewis, D. Neal *et al.*, "Towards expert-level medical question answering with large language models," *arXiv preprint arXiv:2305.09617*, 2023.

[9] I. Nakari and K. Takadama, "Sleep stage estimation by introduction of sleep domain knowledge to ai: Towards personalized sleep counseling system with genai," in *Proceedings of the AAAI Symposium Series*, vol. 3, no. 1, 2024, pp. 368–373.

[10] S. Günay, A. Öztürk, and Y. Yiğit, "The accuracy of gemini, gpt-4, and gpt-4o in ecg analysis: A comparison with cardiologists and emergency medicine specialists," *The American journal of emergency medicine*, vol. 84, pp. 68–73, 2024.

[11] S. Günay, A. Öztürk, H. Özerol, Y. Yiğit, and A. K. Erenler, "Comparison of emergency medicine specialist, cardiologist, and chat-gpt in electrocardiography assessment," *The American Journal of Emergency Medicine*, vol. 80, pp. 51–60, 2024.

[12] L. Zhu, W. Mou, K. Wu, Y. Lai, A. Lin, T. Yang, J. Zhang, and P. Luo, "Multimodal chatgpt-4v for electrocardiogram interpretation: Promise and limitations," *Journal of Medical Internet Research*, vol. 26, p. e54607, 2024.

[13] A. Sano, J. Amores, and M. Czerwinski, "Exploration of llms, eeg, and behavioral data to measure and support attention and sleep," *arXiv preprint arXiv:2408.07822*, 2024.

[14] A. Zaboli, F. Brigo, M. Ziller, M. Massar, M. Parodi, G. Magnarelli, G. Brigiari, and G. Turcato, "Exploring chatgpt's potential in ecg interpretation and outcome prediction in emergency department," *The American Journal of Emergency Medicine*, vol. 88, pp. 7–11, 2025.

[15] V. Vovk, A. Gammerman, and G. Shafer, *Algorithmic learning in a random world*. Springer, 2005, vol. 29.

[16] Y. Ansari, O. Mourad, K. Qaraqe, and E. Serpedin, "Deep learning for ecg arrhythmia detection and classification: an overview of progress for period 2017–2023," *Frontiers in Physiology*, vol. 14, p. 1246746, 2023.

[17] L. Kuhlmann, K. Lehnertz, M. P. Richardson, B. Schelker, and H. P. Zaveri, "Seizure prediction—ready for a new era," *Nature Reviews Neurology*, vol. 14, no. 10, pp. 618–630, 2018.

[18] H. Yue, Z. Chen, W. Guo, L. Sun, Y. Dai, Y. Wang, W. Ma, X. Fan, W. Wen, and W. Lei, "Research and application of deep learning-based sleep staging: Data, modeling, validation, and clinical practice," *Sleep Medicine Reviews*, p. 101897, 2024.

[19] H. Dai, S. Jiang, and Y. Li, "Atrial activity extraction from single lead ecg recordings: Evaluation of two novel methods," *Computers in biology and medicine*, vol. 43, no. 3, pp. 176–183, 2013.

[20] O. Faust, U. R. Acharya, H. Adeli, and A. Adeli, "Wavelet-based ecg processing for computer-aided seizure detection and epilepsy diagnosis," *Seizure*, vol. 26, pp. 56–64, 2015.

[21] R. Avanzato and F. Beritelli, "Automatic ecg diagnosis using convolutional neural network," *Electronics*, vol. 9, no. 6, p. 951, 2020.

[22] D. Luo and X. Wang, "Moderntcn: A modern pure convolution structure for general time series analysis," in *The Twelfth International Conference on Learning Representations*, 2024.

- [23] Y. Wang, Y. Han, H. Wang, and X. Zhang, "Contrast everything: A hierarchical contrastive framework for medical time-series," *Advances in Neural Information Processing Systems*, vol. 36, 2024.
- [24] A. Vaswani, "Attention is all you need," *Advances in Neural Information Processing Systems*, 2017.
- [25] E. Eldele, Z. Chen, C. Liu, M. Wu, C.-K. Kwoh, X. Li, and C. Guan, "An attention-based deep learning approach for sleep stage classification with single-channel eeg," *IEEE Transactions on Neural Systems and Rehabilitation Engineering*, vol. 29, pp. 809–818, 2021.
- [26] H. Li, A. S. Carreon-Rascon, X. Chen, G. Yuan, and A. Li, "Mts-1of: medical time-series representation learning via occlusion-invariant features," *IEEE Journal of Biomedical and Health Informatics*, 2024.
- [27] T. G. Dietterich, R. H. Lathrop, and T. Lozano-Pérez, "Solving the multiple instance problem with axis-parallel rectangles," *Artificial intelligence*, vol. 89, no. 1-2, pp. 31–71, 1997.
- [28] M. Scott, L. Su-In *et al.*, "A unified approach to interpreting model predictions," *Advances in neural information processing systems*, vol. 30, pp. 4765–4774, 2017.
- [29] M. T. Ribeiro, S. Singh, and C. Guestrin, "Why should i trust you?" explaining the predictions of any classifier," in *Proceedings of the 22nd ACM SIGKDD international conference on knowledge discovery and data mining*, 2016, pp. 1135–1144.
- [30] D. J. MacKay, "A practical bayesian framework for backpropagation networks," *Neural computation*, vol. 4, no. 3, pp. 448–472, 1992.
- [31] Y. Gal and Z. Ghahramani, "Dropout as a bayesian approximation: Representing model uncertainty in deep learning," in *international conference on machine learning*. PMLR, 2016, pp. 1050–1059.
- [32] M. Ilse, J. Tomczak, and M. Welling, "Attention-based deep multiple instance learning," in *International conference on machine learning*. PMLR, 2018, pp. 2127–2136.
- [33] Z. Shao, H. Bian, Y. Chen, Y. Wang, J. Zhang, X. Ji *et al.*, "Transmil: Transformer based correlated multiple instance learning for whole slide image classification," *Advances in neural information processing systems*, vol. 34, pp. 2136–2147, 2021.
- [34] J. Ramapuram, F. Danieli, E. Dhekane, F. Weers, D. Busbridge, P. Ablin, T. Likhomanenko, J. Digani, Z. Gu, A. Shidani *et al.*, "Theory, analysis, and best practices for sigmoid self-attention," *arXiv preprint arXiv:2409.04431*, 2024.
- [35] T. M. Cover, *Elements of information theory*. John Wiley & Sons, 1999.
- [36] H. Papadopoulos, K. Proedrou, V. Vovk, and A. Gammerman, "Inductive confidence machines for regression," in *Machine learning: ECML 2002: 13th European conference on machine learning Helsinki, Finland, August 19–23, 2002 proceedings 13*. Springer, 2002, pp. 345–356.
- [37] A. N. Angelopoulos, S. Bates, A. Fisch, L. Lei, and T. Schuster, "Conformal risk control," *arXiv preprint arXiv:2208.02814*, 2022.
- [38] R. F. Barber, E. J. Candes, A. Ramdas, and R. J. Tibshirani, "Conformal prediction beyond exchangeability," *The Annals of Statistics*, vol. 51, no. 2, pp. 816–845, 2023.
- [39] B. Kemp, A. H. Zwinderman, B. Tuk, H. A. Kamphuisen, and J. J. Obery, "Analysis of a sleep-dependent neuronal feedback loop: the slow-wave microcontinuity of the eeg," *IEEE Transactions on Biomedical Engineering*, vol. 47, no. 9, pp. 1185–1194, 2000.
- [40] P. Wagner, N. Strodthoff, R.-D. Bousset, D. Kreiseler, F. I. Lunze, W. Samek, and T. Schaeffter, "Ptb-xl, a large publicly available electrocardiography dataset," *Scientific data*, vol. 7, no. 1, pp. 1–15, 2020.
- [41] E. A. Wolpert, "A Manual of Standardized Terminology, Techniques and Scoring System for Sleep Stages of Human Subjects." *Archives of General Psychiatry*, vol. 20, no. 2, pp. 246–247, 02 1969. [Online]. Available: <https://doi.org/10.1001/archpsyc.1969.01740140118016>
- [42] I. Loshchilov, "Decoupled weight decay regularization," *arXiv preprint arXiv:1711.05101*, 2017.
- [43] OpenAI, "Chatgpt: a large language model," 2023, <https://chat.openai.com>.
- [44] A. Sarraju, D. Bruemmer, E. Van Iterson, L. Cho, F. Rodriguez, and L. Laffin, "Appropriateness of cardiovascular disease prevention recommendations obtained from a popular online chat-based artificial intelligence model," *Jama*, vol. 329, no. 10, pp. 842–844, 2023.
- [45] M. Bilal, Y. Jamil, D. Rana, and H. H. Shah, "Enhancing awareness and self-diagnosis of obstructive sleep apnea using ai-powered chatbots: the role of chatgpt in revolutionizing healthcare," *Annals of Biomedical Engineering*, vol. 52, no. 2, pp. 136–138, 2024.
- [46] P. Wang, S. Bai, S. Tan, S. Wang, Z. Fan, J. Bai, K. Chen, X. Liu, J. Wang, W. Ge *et al.*, "Qwen2-vl: Enhancing vision-language model's perception of the world at any resolution," *arXiv preprint arXiv:2409.12191*, 2024.
- [47] J. Wei, X. Wang, D. Schuurmans, M. Bosma, F. Xia, E. Chi, Q. V. Le, D. Zhou *et al.*, "Chain-of-thought prompting elicits reasoning in large language models," *Advances in neural information processing systems*, vol. 35, pp. 24 824–24 837, 2022.
- [48] P. Lewis, E. Perez, A. Piktus, F. Petroni, V. Karpukhin, N. Goyal, H. Küttler, M. Lewis, W.-t. Yih, T. Rocktäschel *et al.*, "Retrieval-augmented generation for knowledge-intensive nlp tasks," *Advances in Neural Information Processing Systems*, vol. 33, pp. 9459–9474, 2020.